Plasma Chem Plasma Process
DOI 10.1007/s11090-016-9748-8

ORIGINAL PAPER

The Effects of Non-thermal Plasma on the Morphology of Ce-doped ZnO: Synthesis, Characterization and Photocatalytic Activity of Hierarchical Nanostructures

Hadi Fallah Moafi[1] · Mitra Hafezi[1] · Sirous Khorram[2] · Mohammad Ali Zanjanchi[1]

Received: 9 June 2016 / Accepted: 14 September 2016

Abstract ZnO nanoparticles with and without 8 mol % Ce dopant were synthesized by precipitation method and the prepared samples were treated with various types of non-thermal plasma in order to study their effects on the morphology and photocatalytic activity of the samples. As-prepared Ce-doped ZnO has a hexagonal wurtzite structure and the crystal system was not changed by the plasma treatment. The morphology of Ce-doped ZnO was changed from spherical particle to flower and rod-like shapes by the plasma treatment. The particle size of the treated Ce-doped ZnO is smaller in comparison with that of untreated sample. The photodegradation of methylene blue by the plasma-treated Ce-doped ZnO in aqueous solution is higher than that of the untreated Ce-doped ZnO. The enhancement of the photocatalytic activity by the plasma-treated samples may come from the particle size reduction, enhancement in charge separation efficiency and increase of the surface area.

Keywords Ce-doped ZnO · Non-thermal plasma · Morphology · Photocatalysis · Methylene blue

Introduction

In the recent years nanoparticles have gained a lot of attention due to their potential applications in various areas of technology. For example, nanostructured ZnO compounds have attracted great interest in their novel optical, sensor, electronic, mechanical and

✉ Hadi Fallah Moafi
Fallah.m@guilan.ac.ir

[1] Department of Chemistry, Faculty of Science, University of Guilan, P.O. Box 41335-19141, Rasht, Iran

[2] Research Institute for Applied Physics and Astronomy, University of Tabriz, 51666-14766 Tabriz, Iran

Published online: 19 September 2016

photocatalytic properties [1–3]. Unfortunately, ZnO has a drawback in photocatalytic applications, which is due to exhibition of its photoactivity only under ultraviolet light. This is related to its wide band gap (3.37 eV). Also, suppression of the recombination of photogenerated electron–hole pairs will improve the efficiency of photocatalytic activity. Doping with metals or metal oxides is one solution for improving the charge separation and reduction of band gap energy [3].

In recent years, assembling of nanocrystalline structures into the desirable hierarchical nanostructures has attracted much attention due to the size and shape-dependent properties of nanomaterials [4]. The hierarchical nanostructures can be classified into either the structures with nanoscale building blocks extended into more than one dimension or the structures with multiple components which show improved physical and chemical properties for broad applications [5]. Among the various hierarchical nanomaterials, the study of hierarchical semiconductor nanostructures is of particular interest for applications in photocatalysis, solar cells, sensors, adsorption, reduction of metal ions and optical properties [6–12]. In particular, ZnO hierarchical nanostructures have proven to be a potential material for photocatalytic applications.

Several ZnO nanostructures with diverse size and morphology like nanorods [13], nanowires [14], flower-like [15], nanotubes [16], nanosheets [17], nanobelts [18], nanospheres [19], and cabbage-like [20] has been successfully synthesized.

Many methods have been developed to produce ZnO hierarchical nanostructures, such as magnetron sputtering deposition [21], hydrothermal methods [22], template-free chemical method [23], electrochemical deposition [24], microwave treatment [25], and thermal-evaporation process [26]. Recently, the hydrothermal method has become the subject of interest in the synthesis of ZnO hierarchical nanostructures because of its simple procedure, moderate-temperature and low cost. More recently, non-thermal plasma techniques including radio frequency (RF) discharge, glow discharge and silent discharge have been used for surface modification, morphological changes, treatment of wastewater and modification of the activity and stability of catalysts [27–39]. However, there are few reports on the effect of morphological alterations on the catalytic activity of materials. For example, Zen-Hung et al. [28] synthesized the flower-like Ag_2O nanostructures from Ag colloids by O_2 and H_2 plasma treatment and tested it for photocatalytic degradation of methylene blue (MB). Khataee et al. [27] have investigated the conversion of natural zeolite microparticles to nanorod structures by glow discharge plasma. In this work, Ce-doped ZnO was prepared by precipitation method and modified by different non-thermal plasma. The degradation of MB solution by plasma treated Ce-doped ZnO under UV irradiation was performed and compared with the photocatalytic activity of non-treated Ce-doped ZnO. The results show that the plasma treatment improved the photocatalytic activity.

Experimental Section

Chemicals and Materials

All commercial reagents such as zinc sulphate heptahydrate ($ZnSO_4 \bullet 7H_2O$), cerium sulphate tetrahydrate ($Ce(SO_4)_2 \bullet 4H_2O$), sodium hydroxide and methylene blue were analytically pure, purchased from Merck (Germany) and used without further purification. Deionized water was used throughout the study.

Synthesis of the Nanostructures

The ZnO and Ce-doped ZnO nanoparticles were synthesized by simple precipitation method. Zinc sulphate heptahydrate ($ZnSO_4 \bullet 7H_2O$) was used as zinc oxide source. In a typical procedure route for synthesis of the nanostructures, zinc sulphate heptahydrate (0.02 mol) was dissolved in 100 ml of de-ionized water under vigorous stirring at room temperature. Then aqueous solution of sodium hydroxide (0.1 M) was slowly added into the solution under stirring until pH of the solution reached to 12. The white precipitates formed were filtered out and washed several times with deionized water to remove the unreacted reagents. Finally, obtained precipitated solid was dried at 80 °C and then was calcinated at 300 °C for 3 h. For the synthesis of Ce-doped ZnO, cerium sulphate (8 mol % with respect to zinc sulphate) were dissolved in de-ionized water and then the solution was added drop by drop into the aqueous solution of zinc sulphate. Then, solution of sodium hydroxide (0.1 M) was added drop wise into the above prepared solution under stirring until pH of the solution reached to 12. The yellow precipitates formed were filtered and washed with de-ionized water. Subsequently, the prepared precipitates were dried at 80 °C and then calcinated at 300 °C for 3 h.

Plasma Treatment Procedure

The glow discharge plasma system for the plasma treatment of samples is illustrated in Fig. 1. The plasma reactor is made of a Pyrex tube reactor with size of 40 cm × 5 cm. Powder sample (1 g) on the Pyrex plate was placed in the positive column region of the tube and dispersed in the area of 3 × 5 cm^2. Because the plasma has a homogenous

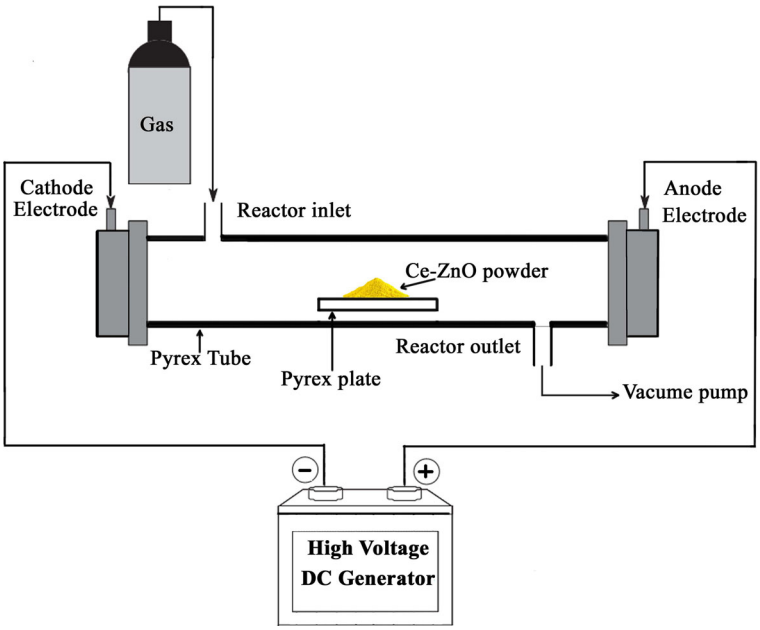

Fig. 1 Schematic diagram of non-thermal plasma experimental setup for treatment of synthesized Ce–ZnO sample

electric field (in the positive column), so, homogeneity of treatment occurs in morphological modification of the catalyst. Different gas plasma was used to modify of the morphology of Ce–ZnO sample. The Pyrex tube was evacuated, and argon, helium, nitrogen or oxygen was introduced into the reactor with keeping the pressure in a range of 25–75 Pa. Then, plasma was generated by applying a high DC voltage (1200–1300 V) [27]. The plasma treatment time ranged from 30 to 60 min. The approximate temperature of the samples after 60 min plasma irradiation was about 45–48 °C. Hereafter, the Ce–ZnO treated with argon, helium, nitrogen and oxygen plasma will be coded as Ce–ZnO–Ar, Ce–ZnO–He, Ce–ZnO–N_2 and Ce–ZnO–O_2, respectively. Then, the photocatalytic efficiency of the obtained samples which suffered various plasma treatments were assessed by measuring the decomposition of MB. In advance of the whole analytical measurement, experiments for obtaining the optimum operating pressure and time were done and revealed that the samples treated under 50 Pa with the plasma treatment time of 30 min showed the highest catalytic activity. So, the feed gas of 50 Pa and the plasma treatment for 30 min were fixed afterward.

Photocatalytic Test

The ultra-violet light photocatalytic activities of non-doped ZnO, untreated and treated Ce–ZnO were evaluated by studying of the photodegradation of MB. Irradiations were carried out using a tube-shaped Krypton lamp (400 W high pressure lamp) with maximum emission at 365 nm without filter which was placed vertically in the reactor. The distance between the lamp and reactor was 40 cm, and the intensity of the UV radiation reaching the reactor was measured to be about 30 mW/cm^2 by a radiometer. The temperature of degradation reaction was kept at 25 °C using a water bath. Prior to the illumination, 50 ml of the MB solution (2×10^{-5} M) containing 40 mg of the samples was stirred for 20 min in dark condition to achieve adsorption–desorption equilibrium between MB and photocatalyst surface. After removing the catalyst from solution by centrifugation, the spectra were measured and the change in absorbance of the MB at its wavelength of maximum absorbance (665 nm) was followed as a function of irradiation time. The concentration of MB was evaluated with a standard calibration curve which was obtained as a relation between the known concentrations in the range of 1×10^{-6}–5×10^{-5} M and the measured absorbance at 665 nm.

Characterization Techniques

X-ray diffraction pattern of samples was carried out at room temperature using a Philips PW1820 X-ray diffractometer with Cupper-Kα radiation operated at 40 kV–30 mA (scan rate being a 0.02°deg./s in 2θ) and within a range of 2θ of 10–70°. The sample morphology was observed by scanning electron microscopy (SEM, Philips XL30) equipped with an EDS attachment for compositional analysis. The population distribution was counted by microstructure measurement software. Zn and Ce contents were determined by ICP-OES (inductively coupled plasma-optical emission spectroscopy). Measurements were made on a ICP-OES Vista-Pro (Varian), after dissolution of the solid samples in a HNO_3:HCl mixture (1/3 ratio). The UV–Vis reflectance spectra were measured with a UV-2100 Shimadzu spectrophotometer attached with an integral sphere in the reflectance mode, using $BaSO_4$ as a reference. The BET surface area of the samples was determined by Sibata SA-1100 surface area analyzer. Photoluminescence spectra (PL) of the samples were carried out by a fluorescence spectrophotometer (Hitachi F-7000). The change of MB

concentration was determined by a RAYLEIGH (UV-1800) ultraviolet–visible scanning spectrophotometer.

Results and Discussion

XRD Analysis

The powder XRD patterns were used to characterize the effects of the addition of Ce on the crystallinity and crystal phase of ZnO. Figure 2 shows the XRD patterns of pure ZnO and Ce–ZnO with various morphologies arose from the plasma treatment (Fig. 3). It can clearly be seen from the XRD profiles that all the samples are highly crystallized. All the peaks can be indexed to the hexagonal wurtzite crystal structure of ZnO. The XRD patterns of all the untreated and plasma treated Ce-doped ZnO are similar to that of pure ZnO, suggesting that there is no change in the crystal structure originated from cerium doping and plasma

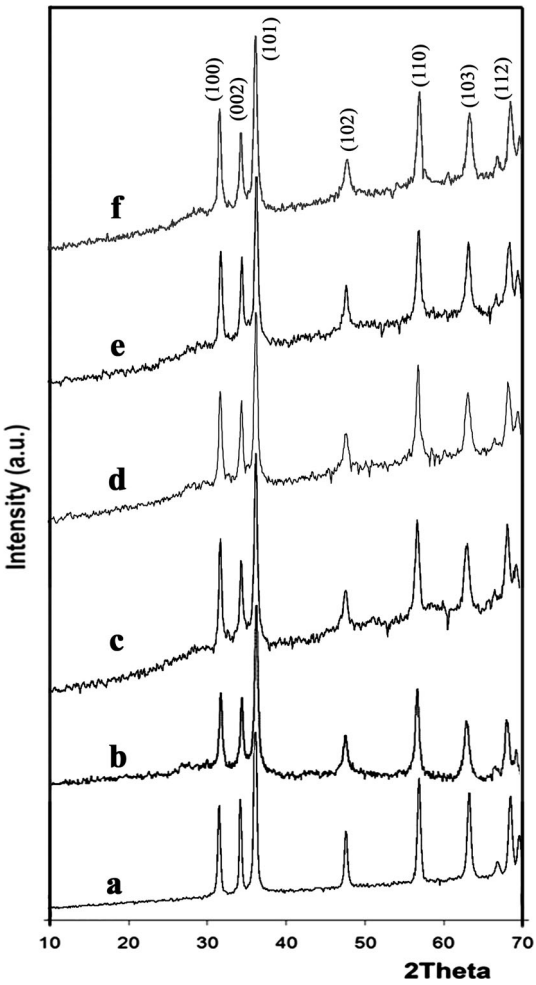

Fig. 2 XRD pattern of undoped ZnO, Ce-doped ZnO and plasma treated Ce-doped ZnO samples: **a** undoped ZnO, **b** Ce-doped ZnO, **c** Ce–ZnO–Ar, **d** Ce–ZnO–He, **e** Ce–ZnO–N_2 and **f** Ce–ZnO–O_2

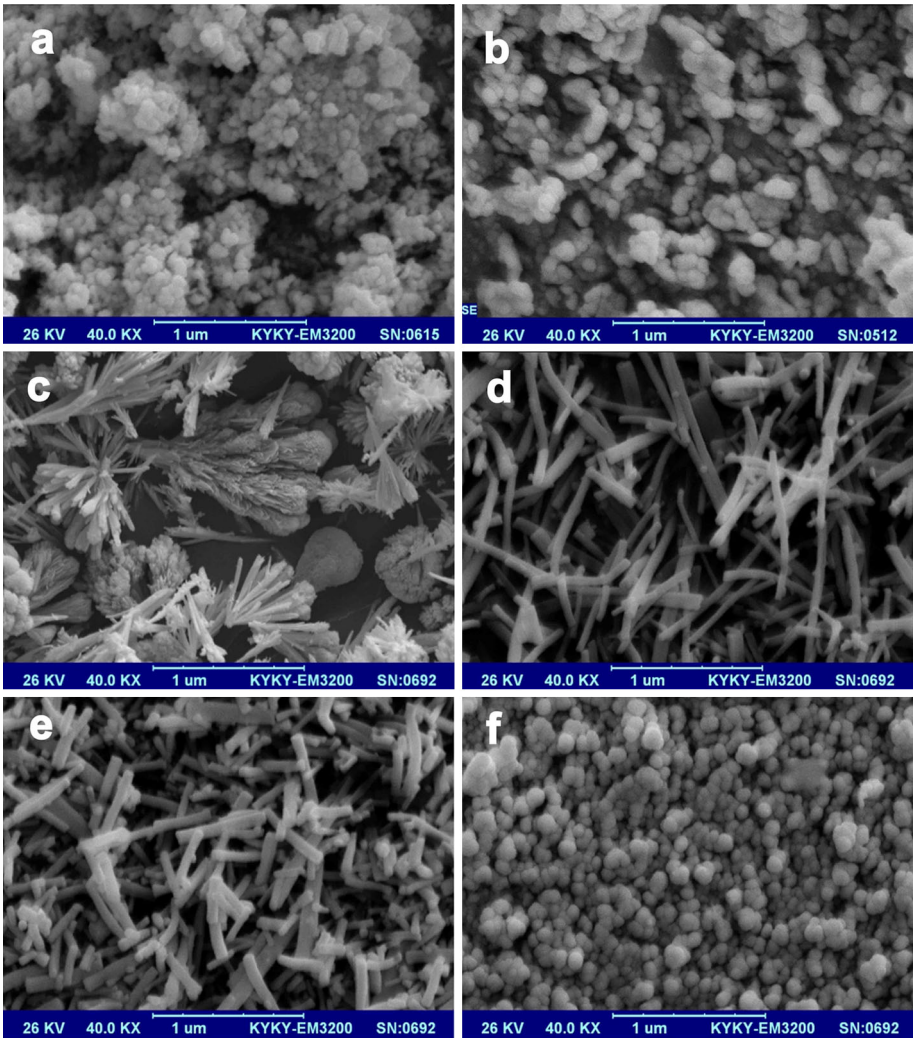

Fig. 3 SEM images of: **a** undoped ZnO, **b** Ce-doped ZnO, **c** Ce–ZnO–Ar, **d** Ce–ZnO–He, **e** Ce–ZnO–N_2 and **f** Ce–ZnO–O_2

treatment processes. However, morphological evidences indicate that as-prepared Ce-doped ZnO nanopowder changed its shape into cauliflower-like or rod-like by the plasma treatment (Fig. 3). These kinds of morphology change demonstrate that the plasma treatment breaks their original structure and constructs different structure even with keeping the original crystal system (hexagonal wrutzite). There were no apparent peaks relating to the separate dopant materials (Ce, CeO_2 and Ce_2O_3). This could be attributed to the fact that the dopant metal/metal oxide was too low in concentration and/or has amorphous structure. The average grain sizes are calculated using the Scherrer's equation from the full width at half maximum of (101) peak and the results are summarized in Table 1. It is interesting to note that the particles size of plasma-treated Ce-doped ZnO is smaller than that of the

Table 1 Some characteristics of ZnO, Ce-doped ZnO and treated Ce–ZnO with different non-thermal plasma

Samples	Crystalline structure	Contents Nominal Ce (mol %)	ICP Ce (mol %)	Absorption edges (nm)	Band gap energy (eV)	BET surface area (m^2/g)	XRD crystal size (nm)	FWHM of (101) peak	SEM average crystal size (nm)
ZnO	Wurtzite	–	–	400	3.10	32.1	40	0.2068	Φ49.5
Ce–ZnO	Wurtzite	8	6.9	470	2.64	38.3	32	0.2558	Φ45.4
Ce–ZnO–Ar	Wurtzite	8	6.5	480	2.58	58.2	21	0.3936	Φ18.2 × 186.8
Ce–ZnO–He	Wurtzite	8	6.8	475	2.61	53.5	21	0.3936	Φ41.6 × 414.2
Ce–ZnO–N_2	Wurtzite	8	6.6	485	2.55	51.8	28	0.2952	Φ38.7 × 256.3
Ce–ZnO–O_2	Wurtzite	8	6.8	470	2.64	48.6	21	0.3936	Φ41.4

untreated Ce-doped and pure ZnO (Table 1), which is consistent with the SEM observation.

Morphology and Compositional Analysis

The surface morphology and composition of the untreated and plasma-treated samples were determined by SEM equipped with EDS analyzer. Figure 3 shows SEM micrographs of ZnO, untreated and plasma-treated Ce-doped ZnO. The particle and diameter size distribution are shown in Fig. 4. Figure 3a is a SEM micrograph of pure ZnO nanoparticles; the most of the nanoparticles have an approximately spherical shape with the average size of Φ49.5 nm (Fig. 3a). Figure 3b shows that surface morphology of untreated Ce–ZnO sample is similar to that of the pure ZnO and the Ce–ZnO nanoparticles were constructed of agglomerates of fine particles with the average size of Φ45.4 nm. SEM image of Ce–ZnO–Ar indicate that the sample consists of massy flower-like (Broccoli-like or Cauliflower) nanostructures (Fig. 3c) consisting of nanorods with an average size of Φ18.2 × 186.8 nm. Ce–ZnO–He is rod-shaped nanocrystals which are distributed spatially in regular direction (Fig. 3d). Nanorods

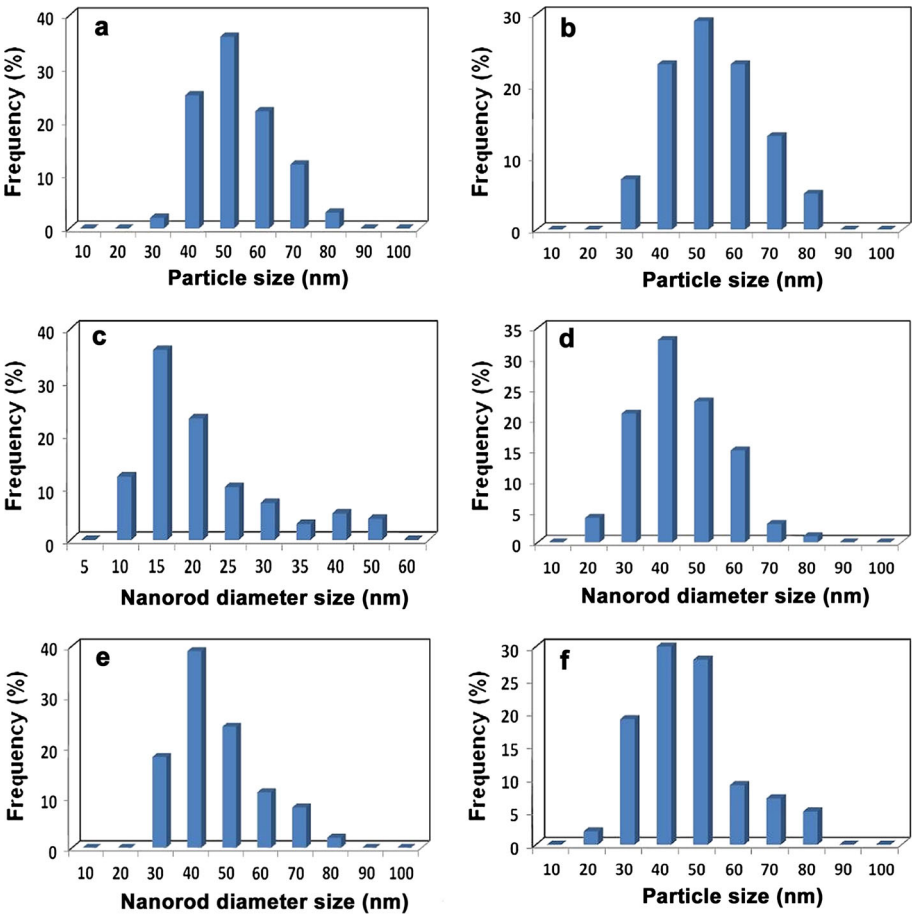

Fig. 4 Particle and diameter size distribution plots of: **a** undoped ZnO, **b** Ce-doped ZnO, **c** Ce–ZnO–Ar, **d** Ce–ZnO–He, **e** Ce–ZnO–N_2 and **f** Ce–ZnO–O_2

of Ce–ZnO–He have an average size of Φ41.6 × 414.2 nm (Fig. 3d). This image confirm that the morphology of Ce–ZnO is completely converted to nanorods crystals after plasma treatment. The Ce–ZnO–N_2 sample shows a similar morphology to the Ce–ZnO–He (Fig. 3e). It can be seen that the Ce–ZnO–N_2 were composed of nanorods with an average size of Φ38.7 × 256.3 nm (Fig. 3e). Ce–ZnO–O_2 is relatively spherical nanoparticles with an average size of Φ41.4 nm (Fig. 3f). On the other hand, it can clearly see that the nanoparticles are well relatively spherical and particles size was changed than that of untreated Ce–ZnO during the oxygen plasma treatment.

To check the chemical composition of the untreated and plasma treated Ce–ZnO samples EDS spectroscopy analysis was performed. Figure 5 shows the EDS analysis of Ce-doped ZnO samples. The existence of the Ce dopant can be clearly observed in the spectra. It was found that the achieved Ce-doped ZnO samples are composed of Zn, O and Ce elements and no other peak is observed, demonstrating the high purity of the Ce–ZnO samples. Since EDS analysis illustrates only elemental composition of single points of catalyst surface, it is not trustworthy. Therefore, the real Ce content in Ce-doped ZnO

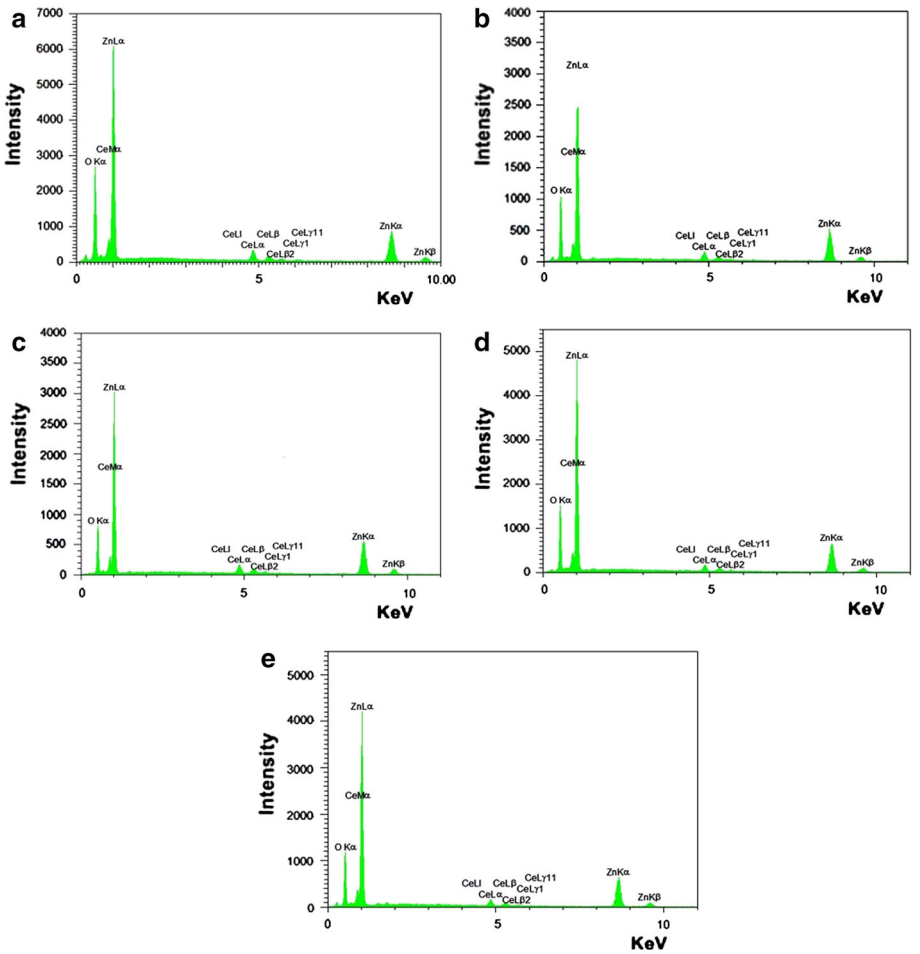

Fig. 5 EDS analysis of: **a** Ce-doped ZnO, **b** Ce–ZnO–Ar, **c** Ce–ZnO–He, **d** Ce–ZnO–N_2 and **e** Ce–ZnO–O_2

samples (8 mol % Ce as nominal) was measured by ICP-OES (Table 1). The values of Ce concentration (mol %) in the Ce–ZnO samples were 6.9, 6.5, 6.8, 6.6 and 6.8 mol % for untreated Ce–ZnO, Ce–ZnO–Ar, Ce–ZnO–He, Ce–ZnO–N_2 and Ce–ZnO–O_2, respectively. It was found that the chemical composition of plasma treated samples is close to the nominal concentration of Ce.

The surface area of undoped ZnO, untreated and treated Ce–ZnO samples was determined using the nitrogen gas adsorption method (Table 1). The results indicate that surface area increased by doping of Ce and plasma treatment. The order of surface area is as follows: Ce–ZnO–Ar > Ce–ZnO–He > Ce–ZnO–N_2 > Ce–ZnO–O_2 > Ce–ZnO > ZnO.

UV–Visible Diffuse Reflectance Spectra

Figure 6 shows the UV–Vis absorption spectra of the samples. The Ce-doped ZnO exhibited a red-shift in the optical absorption band toward the visible regions as compared with the undoped ZnO. It can be said from Fig. 6 that the plasma treatment leads a red-shift in the absorption edge and the increased absorption intensity of the samples. The band gap energy (Eb) of the untreated and plasma-treated Ce-doped ZnO samples can be calculated by the equation, Eb = 1239.8/λ, where λ is the wavelength (nm) of the adsorption edge (Table 1). The optical adsorption edge was obtained from spectra by the intercept on the wavelength axis for a tangent drawn on absorption spectra. Dopant-induced red shift and increased absorption can arise the improved formation rate of e^-/h^+ pairs, which may result in higher activity of the photocatalyst [40].

Photoluminescence (PL) Study

PL spectra of the samples are measured with an excitation wavelength of 370 nm at room temperature are shown in Fig. 7. The PL spectrum of pure ZnO nanostructure consists of a band edge emission around 410 nm and defect-state emission bands around 460 nm

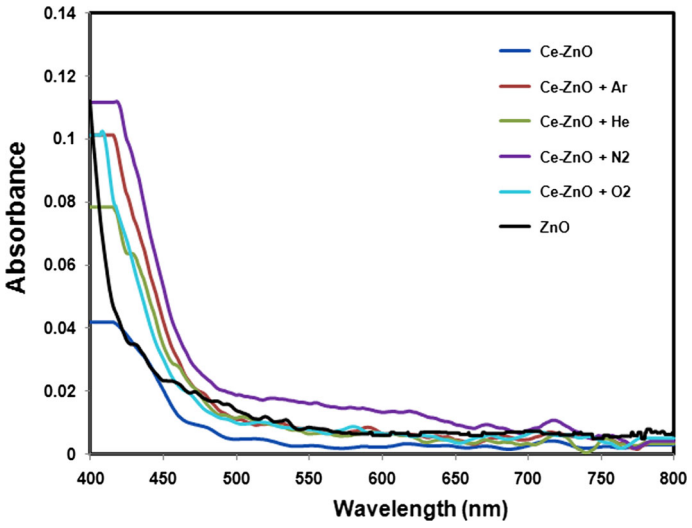

Fig. 6 Diffuse reflectance spectra of synthesized ZnO and Ce-doped ZnO and treated Ce–ZnO with different non-thermal plasma

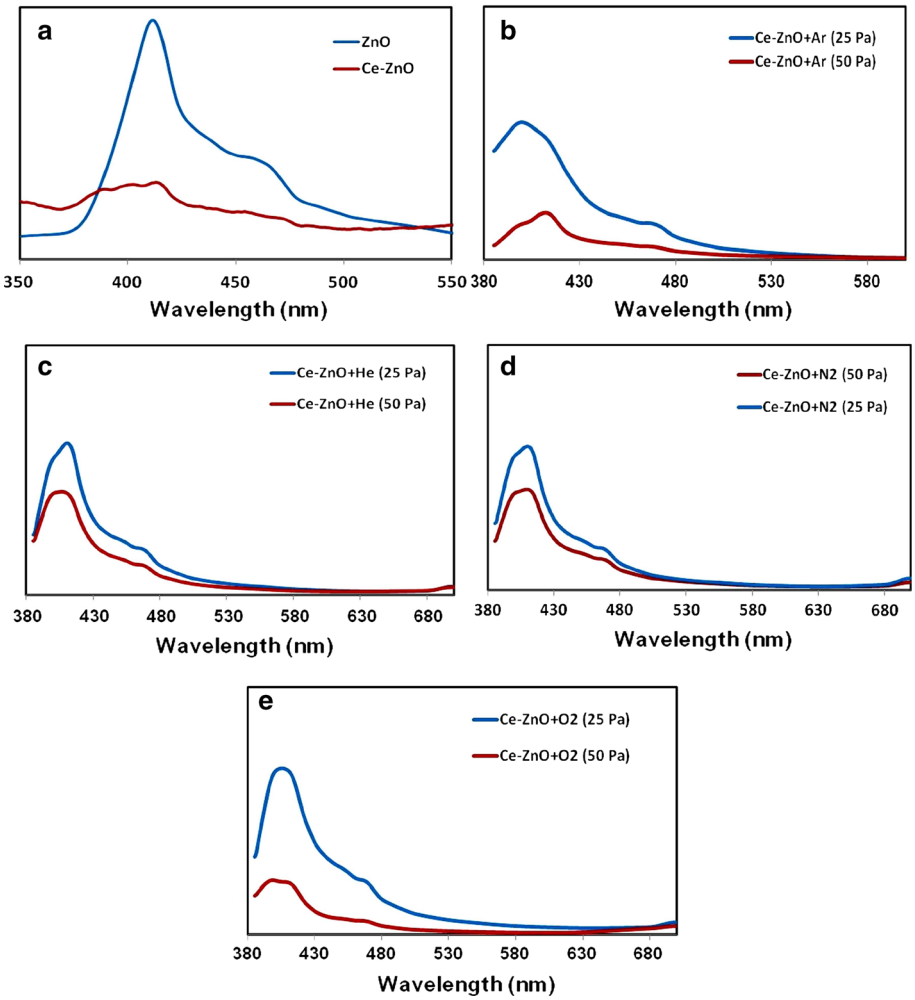

Fig. 7 PL spectra of: **a** ZnO and Ce-doped ZnO, **b** Ce–ZnO–Ar (at 25 and 50 Pa), **c** Ce–ZnO–He (at 25 and 50 Pa), **d** Ce–ZnO–N_2 (at 25 and 50 Pa) and **e** Ce–ZnO–O_2 (at 25 and 50 Pa)

(Fig. 7a). These peaks are attributed due to the presence of various types of defects in the as-prepared ZnO. The probable defects can be interstitial Zn or O (Zn_i or O_i), zinc vacancy (V_{Zn}) or the oxygen antisite (O_{Zn}) [41, 42]. It is obvious that the increasing of Ce significantly decreases the PL intensity. The Ce centers in Ce–ZnO act as traps to the excited electrons thus reduce the PL efficiency. Decreased UV emission was considered due to the increase of the nanoradiative defects and decrease of Ce–ZnO nano size. The PL spectra of plasma-treated Ce-doped ZnO nanostructures at two different pressures are shown in Fig. 7b–e. It was found that the shape of the spectrum of the plasma-treated Ce-doped ZnO were similar even with different treatment pressure, but the PL intensity of the samples treated with any type of plasma with a higher pressure becomes lower. The lower PL emission for the plasma-treated Ce–ZnO samples suggests that the recombination of electrons and holes is greatly prevented. The mechanism will be discussed with the photocatalytic activity results in the next section again.

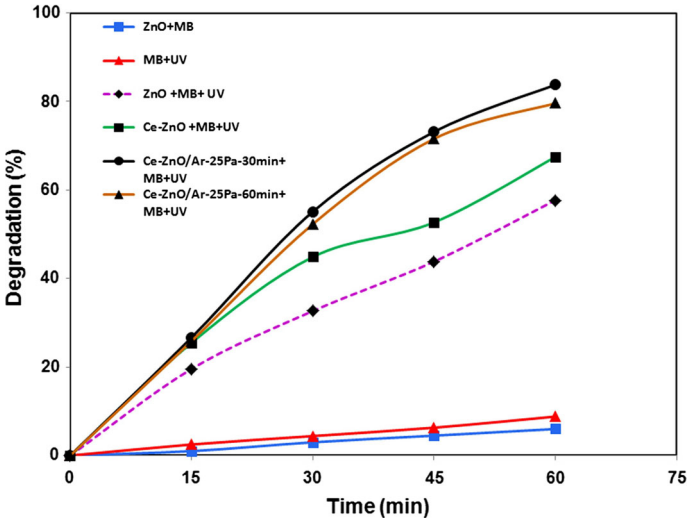

Fig. 8 Photodegradation of MB in absence and presence of ZnO and also in presence of Ce–ZnO and argon-treated Ce–ZnO at 25 Pa and different time under UV irradiation (Experimental conditions: pH = 7, catalyst weight = 40 mg, dye concentration = 2×10^{-5} M and temperature = 25 °C)

Evaluation of Photocatalytic Activity

Photodegradability of Methylene Blue

The photocatalytic performance of the samples has been evaluated for the degradation of MB (Fig. 8). The MB was not decomposed by UV irradiation in the absence of ZnO. When UV light was not irradiated, the MB was stable but adsorbed a little. It was observed that photoactivity of Ce–ZnO is higher than that of pure ZnO. Figure 8 indicates that the doping of Ce into ZnO improves the photocatalytic efficiency and this fact suggests that Ce doping might create the trap centers for electrons or holes [43]; this result on the photocatalytic activity study is consistent with the results obtained in the PL study.

Effect of Plasma Treatment

To evaluate the photoactivity of the plasma treated Ce-doped ZnO and determine the optimum conditions of plasma treatment, photodegradation experiments on MB were carried out by Ce–ZnO samples modified by Ar plasma. The results are given in Figs. 8 and 9. It is found from Fig. 8 that, the photocatalytic activity of the treated Ce–ZnO is higher than that of untreated Ce–ZnO. Also, time of 30 min treatment is better than 60 min treatment. So, 30 min time was selected as the optimum time for all the experiments.

Effect of Plasma Gas Pressure

In order to study the effect of plasma gas pressure on the photocatalytic activity, the Ce–ZnO samples were treated at 25, 50 and 75 Pa for 30 min. It is clear that from Fig. 9, photodegradation of MB enhances with increasing of plasma gas pressure. In the other hand, the MB degradation by the Ce–ZnO treated at plasma gas pressure of 50 Pa is higher

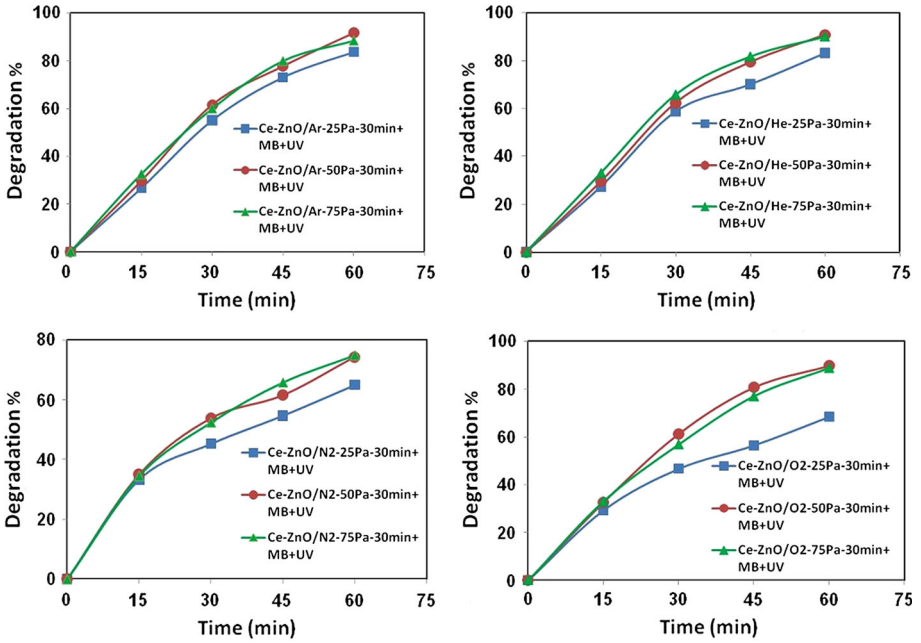

Fig. 9 Photodegradation of MB in presence of treated Ce–ZnO by different gas at different pressure (25, 50 and 75 Pa) for 30 min under UV irradiation (Experimental conditions: pH = 7, catalyst weight = 40 mg, treatment time = 30 min, dye concentration = 2×10^{-5} M and temperature = 25 °C)

than that at 25 Pa and the photocatalytic activity of the samples treated at 75 Pa is almost the same as that at 50 Pa. It can be thought from these results that the effect of plasma gas pressure on the photocatalytic activity might reach the upper limit at 50 Pa. Therefore, 50 Pa of plasma gas pressure is adopted for the optimum experimental condition.

Effect of Photocatalyst Weight

Photoactivity of semiconductor materials strongly depends on catalyst weight. The effect of weight of plasma-treated Ce–ZnO samples on the degradation of MB was evaluated in the range of 40–80 mg at pH = 7 and with constant dye concentration of 2×10^{-5} M. As shown in Fig. 10, the photodegradation of MB enhances with increasing of photocatalyst weight from 40 to 80 mg at 60 min degradation time. It is clear that from Fig. 10, the MB degradation by the treated Ce–ZnO by catalyst dose of 60 mg is higher than that at 40 mg and the photocatalytic activity of the samples at 80 mg is almost the same as that at 60 mg. It can be concluded from these results that the effect of catalyst weight on the photocatalytic activity might reach the upper limit at 60 mg. Therefore, 60 mg of catalyst weight is adopted as the suitable dosage for the all experiments.

Effect of Solution pH

The effect of pH on photocatalytic activity of MB was examined by keeping all other experimental conditions in the range of 3, 7 and 10. As can be seen in Fig. 11, the degradation efficiency was abruptly decreased in solutions in acidic pH. The decline in the

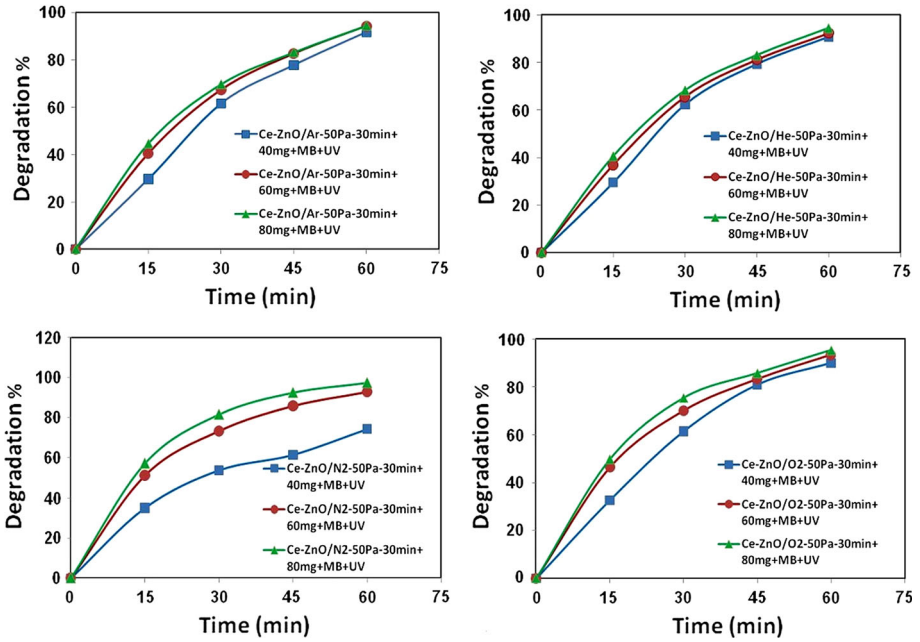

Fig. 10 Photodegradation of MB in presence of different amount of plasma treated Ce–ZnO by different plasma under UV irradiation (Experimental conditions: pH = 7, pressure = 50 Pa, treatment time = 30 - min, dye concentration = 2×10^{-5} M and temperature = 25 °C)

photodegradation in acidic pH may be due to dissolution or photodecomposition of Ce–ZnO. The high degradation was achieved to be at pH 10. The highest degradation rate at pH 10 and decreased rates at lower pH might be ascribed to the fact that the isoelectric point of ZnO is 8.7–10.3 [44]. The electrostatic neutrality may increase the adsorption of MB and increase the photodegradation.

Effect of Initial Concentration of Methylene Blue

The photodecomposition of MB was performed at initial concentrations of 1×10^{-5} (not shown in Fig. 12), 2×10^{-5} and 3×10^{-5} M. It was observed in advance that the degradation ratio of MB at the initial concentration of 1×10^{-5} M is similar to that of 2×10^{-5} M by 15 min UV-irradiation. Because the change in absorption is larger in 2×10^{-5} M than 1×10^{-5} M, 2×10^{-5} M results was drown with 3×10^{-5} M results in Fig. 12. When the initial concentration increased by 3×10^{-5} M, the degradation ratio decreased from the 2×10^{-5} M case; this may come from the UV-light shadowing effect by MB itself (Fig. 12). Then, it is concluded that 2×10^{-5} M initial concentration of the MB is the optimum.

Reusability of Catalyst

The durability of the photocatalysts is very important for practical applications. In order to investigate reusability and stability of the Ce-doped ZnO photocatalyst, the photodegradation experiments were carried out in optimized conditions (temperature = 25 °C, catalyst weight = 60 mg, dye concentration of 2×10^{-5} M and pH = 10). In the

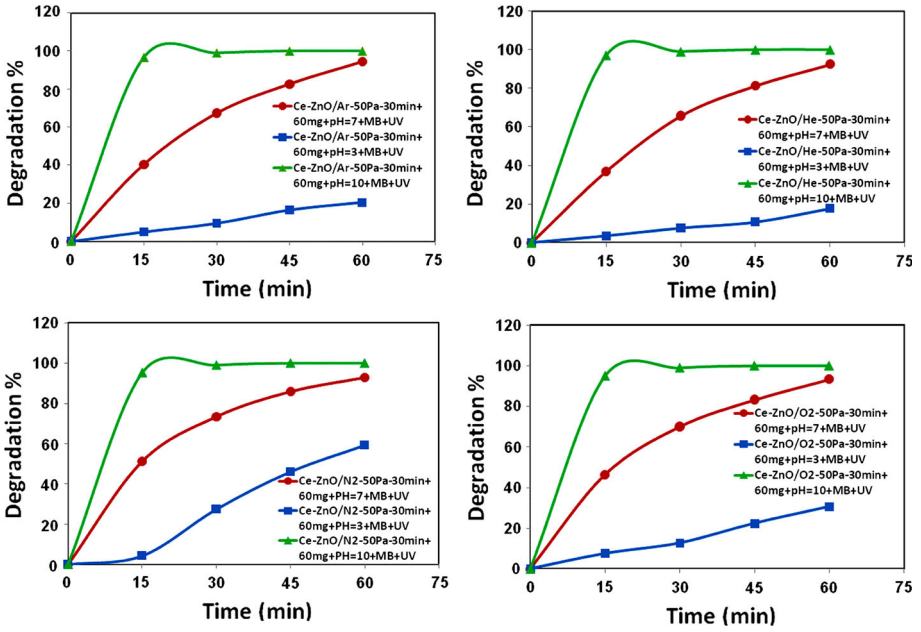

Fig. 11 Effect of pH on the photocatalytic degradation of MB in presence plasma treated Ce–ZnO samples (Experimental conditions: catalyst weight = 60 mg, pressure = 50 Pa, treatment time = 30 min, dye concentration = 2×10^{-5} M and temperature = 25 °C)

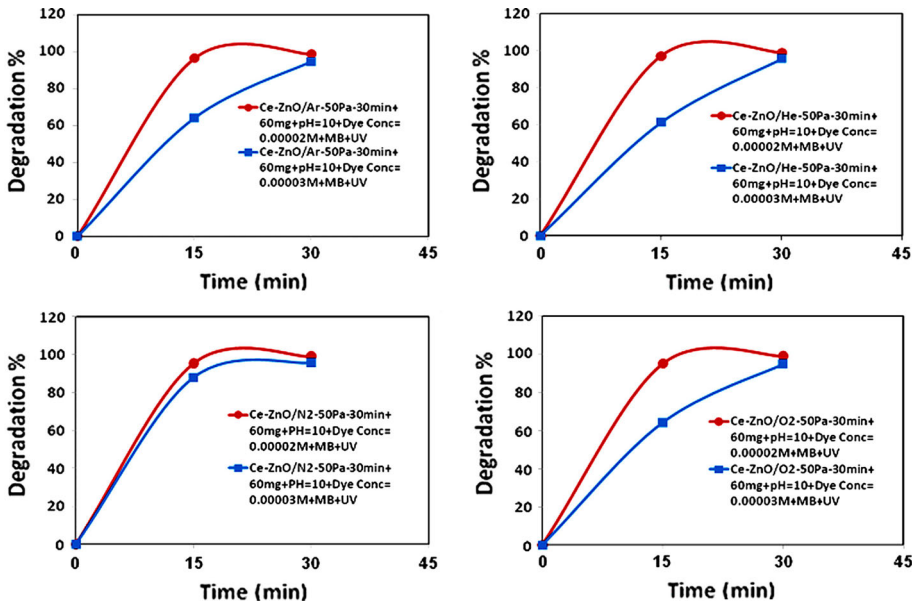

Fig. 12 The Effect of initial dye concentration on the photocatalytic degradation of MB in presence of plasma treated Ce–ZnO samples (Experimental conditions: catalyst weight = 60 mg, pressure = 50 Pa, treatment time = 30 min, pH = 10 and temperature = 25 °C)

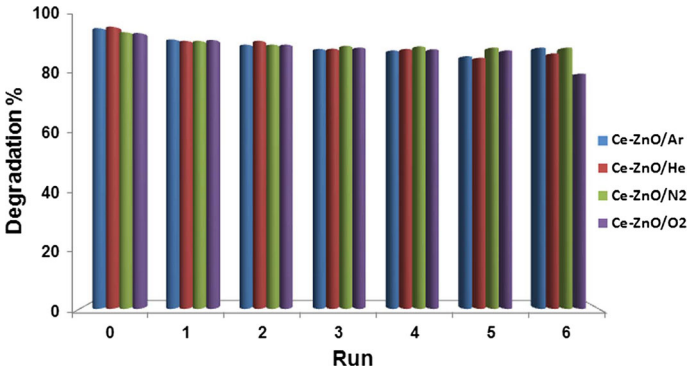

Fig. 13 Plot of degradation percent for MB on the plasma-treated Ce-doped ZnO nanostructures at optimized conditions versus number of runs

experiments, the used treated Ce–ZnO samples were washed with de-ionized water and dried at 50 °C for 12 h and used again. Figure 13 shows the result of the degradation tests using the recycled Ce-doped ZnO for six times. It can be seen that the photocatalytic activity of the plasma-treated Ce-doped ZnO nanostructures did not decrease noticeably throughout the whole six cycles of degradation tests. The results indicate that the Ce–ZnO was reasonably stable under the circumstances used in this research.

Conclusion

ZnO and Ce-doped ZnO nanoparticles were prepared by precipitation method and Ce-doped ZnO were modified by different non-thermal plasma. The Physical and chemical properties of the plasma-treated Ce–ZnO samples were analyzed by XRD, SEM, EDX, ICP-OES, DRS, BET and PL analysis. XRD results confirmed that the crystal system of the modified samples was not changed during the plasma treatment. SEM images showed that the morphology of the Ce–ZnO sample was completely changed to nanoflower by Ar plasma and nanorod-like by He and N_2 plasma treatment. However, O_2 plasma did not change the nanoparticle shape of Ce-doped ZnO but to reduce their size slightly. The photocatalytic performance of untreated and plasma-treated Ce–ZnO samples indicated that the dye elimination efficiency was increased. In order to obtain maximum degradation efficiency, effect of various parameters such as plasma gas pressure, catalyst loading, pH and initial concentration of dye on the degradation of MB on Ce-doped ZnO nanostructures was carried out. The amount of catalyst for plasma-treated Ce-doped ZnO samples was found to be suitable with 60 mg. The degradation of MB was found to be effective in the basic pH range. The repeatability of photocatalytic activity of plasma-treated Ce-doped ZnO was also tested.

Acknowledgments The research was supported by University of Guilan. The authors are highly thankful to University of Guilan for providing financial assistance of this research project.

References

1. Jr AF, Pessoni HVS (2015) Enhanced dielectric constant of Co-doped ZnO nanoparticulate powders. Phys B 476:12–18

2. Shash NM, Ahmed IS (2013) Structure and electrical properties of ZnO doped barium-metaphosphate glasses. Mater Chem Phys 137:734–741
3. Moafi HF, Zanjanchi MA, Shojaie AF (2013) Tungsten-doped ZnO nanocomposite: synthesis, characterization, and highly active photocatalyst toward dye photodegradation. Mater Chem Phys 139:856–864
4. Zhu YF, Zhou GH, Ding HY, Liu AH, Lin YB, Li NL (2010) Controllable synthesis of hierarchical ZnO nanostructures via a chemical route. Physica E 42(9):2460–2465
5. Ren Z, Guo Y, Liu C, Gao P (2013) Hierarchically nanostructured materials for sustainable environmental applications. Front Chem 1:1–22
6. Li X, Yu J, Jaroniec M (2016) Hierarchical photocatalysts. Chem Soc Rev 45:2603–2636
7. Gu J, Li S, Wang E, Li Q, Sun G, Xu R, Zhang H (2009) Single-crystalline α-Fe_2O_3 with hierarchical structures: controllable synthesis, formation mechanism and photocatalytic properties. J Solid State Chem 182:1265–1272
8. Zhang J, Yang Y, Jiang F, Li J, Xu B, Wang S, Wang X (2006) Fabrication of semiconductor CdS hierarchical nanostructures. J Cryst Growth 293:236–241
9. Miles DO, Lee CS, Cameron PJ, Mattia D, Kim JH (2016) Hierarchical growth of TiO_2 nanosheets on anodic ZnO nanowires for high efficiency dye-sensitized solar cells. J Power Sources 325:365–374
10. Zhang S, Li J, Wen T, Xu J, Wang X (2013) Magnetic Fe_3O_4@NiO hierarchical structures:preparation and their excellent As (V) and Cr(VI) removal capabilities. RSC Adv 3:2754–2764
11. Zheng Y, Luo C, Liu L, Yang Z, Ren S, Cai Y, Xiong J (2016) Synthesis of hierarchical TiO_2/SnO_2 photocatalysts with different morphologies and their application for photocatalytic reduction of Cr(VI). Mater Lett 181:169–172
12. Ma Q, Lv X, Wang Y, Chen J (2016) Optical and photocatalytic properties of Mn doped flower-like ZnO hierarchical structures. Opt Mater 60:86–93
13. Shi R, Yang P, Dong X, Ma Q, Zhang A (2013) Growth of flower-like ZnO on ZnO nanorod arrays created on zinc substrate through low-temperature hydrothermal synthesis. Appl Surf Sci 264:162–170
14. Chang Y (2014) Low temperature growth of ZnO nanowire arrays with enhanced high performance photocatalytic activity and reusability. Catal Commun 56:45–49
15. Kilic B, Gunes T, Besirli I, Sezginer M, Tuzemen S (2014) Construction of 3-dimensional ZnO-nanoflower structures for high quantum and photocurrent efficiency in dye sensitized solar cell. Appl Surf Sci 318:32–36
16. Roza L, Rahman MYA, Umar AA, Salleh MM (2015) Direct growth of oriented ZnO nanotubes by self-selective etching at lower temperature for photo-electrochemical (PEC) solar cell application. J Alloys Compd 618:153–158
17. Algarni H, El-Gomati M, Al-Assiri MS (2012) Low-temperature growth and properties of nanocrystalline thin ZnO nanosheet interconnects on zinc foil. Sci Adv Mater 4:961–968
18. Sun T, Qiu J, Liang C (2008) Controllable fabrication and photocatalytic activity of ZnO nanobelt arrays. J Phys Chem C 112:715–721
19. Xu J, Liu C, Wu Z (2011) Direct electrochemistry and enhanced electrocatalytic activity of hemoglobin entrapped in graphene and ZnO nanosphere composite film. Microchim Acta 172:425–430
20. Tarwal NL, Jang JH, Gang MG, Kim JH, Patil PS (2013) The beauty of heterogeneity spray, pyrolyzed Sn–ZnO thin films with cabbage-like morphology. Mater Today 16:403–404
21. Kang SW, Mohanta SK, Kim YY, Cho HK (2008) Realization of vertically well-aligned ZnO: Ga nanorods by magnetron sputtering and their field emission behavior. Cryst Growth Des 8:1458–1460
22. Kim D, Huh Y (2011) Morphology-dependent photocatalytic activities of hierarchical microstructures of ZnO. Mater Lett 65:2100–2103
23. Zhou H, Zhang H, Wang Y, Miao Y, Gu L, Jiao Z (2015) Self-assembly and template-free synthesis of ZnO hierarchical nanostructures and their photocatalytic properties. J Colloid Interface Sci 448:367–373
24. Miculescu F, Rusen E, Mocanu A, Diacon A, Birjega R (2013) Hierarchical nanostructures of ZnO obtained in the presence of water soluble polymers. Powder Technol 239:56–58
25. Hamedani NF, Mahjoub AR, Khodadadi AA, Mortazavi Y (2011) Microwave assisted fast synthesis of various ZnO morphologies for selective detection of CO, CH_4 and ethanol. Sens Actuators, B 156:737–742
26. Fan D, Zhang R, Wang X (2010) Synthesis and optical property of ZnO nanonail arrays with controllable morphology. Physica E 42:2081–2085
27. Khataee A, Bozorg S, Khorram S, Fathinia M, Hanifehpour Y, Joo SW (2013) Conversion of natural clinoptilolite microparticles to nanorods by glow discharge plasma: a novel Fe-impregnated nanocatalystforthe heterogeneous fenton process. Ind Eng Chem Res 52:18225–18233

28. Yang Z, Ho C, Lee S (2015) Plasma-induced formation of flower-like Ag_2O nanostructures. Appl Surf Sci 349:609–614
29. Rahemi N, Haghighi M, Babaluo AA, Jafari MF, Khorram S (2013) Non-thermal plasma assisted synthesis and physicochemical characterizations of Co and Cu doped Ni/Al_2O_3 nanocatalysts used for dry reforming of methane. Int J Hydrog Energy 38:16048–16061
30. He D, Sun Y, Xina L, Feng J (2014) Aqueous tetracycline degradation by non-thermal plasma combined with nano-TiO_2. Chem Eng J 258:18–25
31. Zhu B, Jang BWL (2014) Insights into surface properties of non-thermal RF plasmas treated Pd/TiO_2 in acetylene hydrogenation. J Mol Catal A: Chem 395:137–144
32. Cámara RM, Crespo E, Portela R, Suárez S, Bautista L, Gutiérrez-Martín F, Sánchez B (2014) Enhanced photocatalytic activity of TiO_2 thin films on plasma-pretreated organic polymers. Catal Today 230:145–151
33. Tian M, Batty S, Shang C (2013) Synthesis of nanostructured carbons by the microwave plasma cracking of methane. Carbon 51:243–248
34. Liu C, Zou J, Yu K, Cheng D, Han Y, Zhan J, Ratanatawanate C, Jang BWL (2006) Plasma application for more environmentally friendly catalyst preparation. Pure Appl Chem 78:1227–1238
35. Mok YS, Koh DJ, Kim KT, Nam IS (2003) Non thermal plasma-enhanced catalytic removal of nitrogen oxides over V_2O_5/TiO_2 and Cr_2O_3/TiO_2. Ind Eng Chem Res 42:2960–2967
36. Durme JV, Dewulf J, Leys C, Langenhove HV (2008) Combining non-thermal plasma with heterogeneous catalysis in waste gas treatment: a review. Appl Catal B Environ 78:324–333
37. Tang S, Lu N, Wang JK, Ryu S, Choi H (2007) Novel effects of surface modification on activated carbon fibers using a low pressure plasma treatment. J Phys Chem 111:1820–1829
38. Liu C, Cheng D, Zhang Y, Yu K, Xia Q, Wang J, Zhu X (2004) Remarkable enhancement in the dispersion and low-temperature activity of catalysts prepared via novel plasma reduction − calcination method. Catal Surv Asia 8:111–118
39. Wang R, Hsu C, Chen S (2012) Hydrogen-plasma-assisted growth of anatase TiO_2 nanoneedles on Ti plates. Ind Eng Chem Res 51:3677–3681
40. Chang C, Lin C, Hsu M (2014) Enhanced photocatalytic activity of Ce-doped ZnO nanorods under UV and visible light. J Taiwan Inst Chem Eng 45(4):1954–1963
41. George A, Sharma SK, Chawla S, Malik MM, Qureshi MS (2011) Detailed of X-ray diffraction and photoluminescence studies of Ce doped ZnO nanocrystals. J Alloys Compd 509:5942–5946
42. Wang Y, Yang J, Li Y, Jiang T, Chen J, Wang J (2015) Controllable preparation of ZnO nanostructure using hydrothermal-electrodeposited method and its properties. Mater Chem Phys 153:266–273
43. Kumar R, Umar A, Kumar G, Akhtar MS, Wang Y, Kim SH (2015) Ce-doped ZnO nanoparticles for efficient photocatalytic degradation of direct red-23 dye. Ceram Int 41:7773–7782
44. George AP (1965) The isoelectric points of solid oxides, solid hydroxides, and aqueous hydroxo complex systems. Chem Rev 65:177–198